CIRP Annals - Manufacturing Technology 72 (2023) 129–132

Contents lists available at ScienceDirect

CIRP Annals - Manufacturing Technology

journal homepage: https://www.editorialmanager.com/CIRP/default.aspx

Fatigue prediction and life assessment method for metal laser powder bed fusion parts

Wessel W. Wits (2)[a,b,*], Emiel Amsterdam[c]

[a] Mechanical & Electrical Engineering Department, Thales Nederland B.V., Hengelo, the Netherlands
[b] Faculty of Electrical Engineering, Mathematics and Computer Science, University of Twente, Enschede, the Netherlands
[c] NLR – Royal Netherlands Aerospace Centre, Marknesse, the Netherlands

ARTICLE INFO

Article history:
Available online 8 April 2023

Keywords:
Additive manufacturing
Fatigue
Laser powder bed fusion

ABSTRACT

In this paper, an industry-accepted fatigue model based on generalized stress-life (S–N) curves is adapted for metal parts fabricated by laser powder bed fusion (LPBF). Initial defects inherent to the fabrication process, such as part porosity, are related to fatigue life performance. Hereto, additively manufactured test specimens are fatigue tested and used to formulate a function to predict fatigue life based on the size of initial defects. The predictions correlate well with experimental results and provide a quality measure to expel outliers. The method can be used to predict the life expectancy of LPBF parts based on a priori detected defect sizes.

1. Introduction

Additive manufacturing (AM), colloquially also known as 3D printing, has seen substantial growth over the last decades and has become an industry-accepted fabrication technique [1]. With improving manufacture characteristics, AM developed from rapid prototyping and tool making to part and product fabrication. For metallic parts, laser powder bed fusion (LPBF) is *the* most commonly used fabrication process [2]. Industry uptake of metal LPBF is however generally limited to static and non-critically-loaded components. For critically loaded components, in which the fatigue strength must be assessed, the application of metal LPBF is yet too unreliable [3]. Intrinsic defects inside LPBF parts lead to local stress concentrations and high scatter in fatigue life data thus hampering the assessment of parts' structural integrity over life [4]. Although defect detection has been widely reported upon, the impact on fatigue performance has yet to be elucidated.

Parts fabricated by LPBF typically exhibit two types of intrinsic defects: (i) lack-of-fusion defects caused by insufficient laser penetration or energy, and (ii) entrapped-gas defects caused by vapour recoil or keyhole collapse during melt pool formation [5,6]. Lack-of-fusion defects are generally irregularly shaped and sometimes even include unmolten or partially molten powder particles, while defects due to gas entrapment are generally spherical and small in size. Both types of defects are known to serve as crack nucleation sites [7]. Moreover, irregular-shaped pores are recognized as key contributors to fatigue failure, due to increased local stress concentrations near the defect. As both types of defect are inherent to LPBF, their manifestation is minimized by carefully optimizing the laser process conditions [8]. Post-process quality control methods are intended to assess the size and number of defects; e.g. by destructive testing of co-fabricated witness samples or non-destructive testing by X-ray computed tomography (XCT). As defects are inherent, this paper proposes a method to predict fatigue life of LPBF parts.

The industry-accepted approach to quantifying metal fatigue is the stress-life (S–N) method. This method is primarily useful when parts are loaded in the elastic region, plastic strain is assumed small and the number of cycles to failure is high [9]. The associated S–N curves, or Wöhler diagrams, are widely taught at engineering schools. Next to intrinsic material properties, it is well known that e.g. a part's surface finish (i.e. the surface roughness) plays a dominant role in its fatigue life. This is illustrated in Fig. 1(a) in which three generalized S–N curves that are based on empirical relations are shown. The endurance limit, S_e, is projected at 10^6 cycles after which infinite life is assumed. The maximum alternating stress at the endurance limit is determined experimentally. For the same material, a higher surface roughness will lower the maximum alternating stress at the

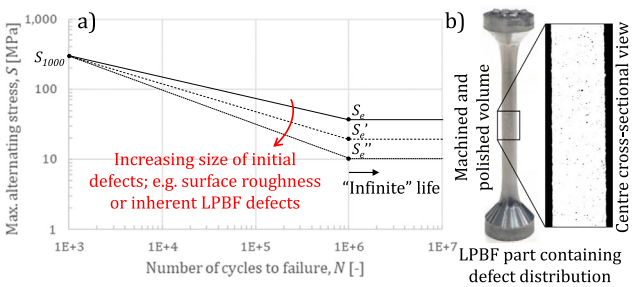

Fig. 1. Generalized S–N curves with changing slope from S_{1000} for increasing initial defect sizes (a). Exemplary LPBF part with intentionally designed defects used for fatigue testing and life prediction (b).

* Corresponding author.
E-mail address: wessel.wits@nl.thalesgroup.com (W.W. Wits (2)).

https://doi.org/10.1016/j.cirp.2023.03.011

endurance limit as indicated by the red arrow. At 1000 cycles however, the alternating stress is assumed to be independent of the surface roughness [9]. Hence for similar materials, the S–N curves converge to a single point: S_{1000}. Hence, S_{1000} acts as a pivot point and together with S_e, the S–N curve can be expressed as:

$$N = 1000\left(\frac{S}{S_{1000}}\right)^{n} \text{ with } n = \frac{3}{\log_{10}\left(\frac{k_s S_e}{S_{1000}}\right)} \quad (1)$$

where k_s is the surface factor and S_e the maximum alternating stress at the endurance limit for parts with a mirror-polished surface finish. For steel, S_{1000} and S_e are typically at about 90% and 50% of the Ultimate Tensile Strength (UTS), respectively, and literature provides surface factors that are multiplied with S_e to lower the maximum alternating stress at the endurance limit to e.g. S_e' and S_e" as illustrated in Fig. 1(a) [9,10]. As such, the S_{1000} method is a well-known empirical method that takes the surface roughness into account by effectively changing the slope n in Eq. (1) through the surface factor [10].

In this paper, we propose an adjustment of the S_{1000} method by assuming that the size of intrinsic LPBF defects act similarly as surface roughness and result in a change in slope of the S–N curve [9]. Fabricated test specimens with known defects, as shown in Fig. 1(b), are used to quantify S–N curves specifically for fatigue prediction of LPBF parts. By experimentally determining the slope n and finding the pivot point where defect sizes are insignificant for fatigue life, the endurance limit of LPBF parts of which initial defects sizes are known a priori can be predicted.

2. Methodology

To determine S–N curves correlated to inherent LPBF defect sizes, an extensive experimental test campaign was performed. 78 test specimens, similar to Fig. 1(b), were fabricated using LPBF in three consecutive builds. Six specimen types were defined in which each type exhibits different internal defects by adjusting the laser scan strategy. Fabrication was done using an SLM solutions 280 HL system. AlSi10Mg was selected as feedstock material, as this material has interesting use for lightweight, structural components that are required to withstand high loads. The test specimens were printed vertically with respect to the build plate and had a cylindrical shape. The vertical direction typically shows the lowest fatigue strength, due to the fact that lack-of-fusion defects occur between build layers and hence parts consisting of more layers statistically show more of such defects [11]. The as-built gauge section was Ø4 × 18 mm in length. After a 2 h 300 °C stress relieve heat treatment, the test specimens were machined and polished to the final gauge diameter of Ø3 mm. Polishing down to Ra ≤ 0.2 µm was performed to minimize surface roughness effects and have LPBF defects prevail in the fatigue assessment.

The six specimen types, including the LPBF process parameters used to create intentional defects, were introduced in an earlier study [5]. For the sake of brevity, here only the defect types are discussed. Type A is built according to the material-specific optimized parameter set focused on minimal porosity and should thus give best fatigue results. The gauge section of these test specimens is built by a hatch pattern; hence, only hatch defects should be present in the built specimens. Specimen types B, C and D are designed to feature inherent LPBF defects by adjusting the process settings of the laser skin passes surrounding a core hatched region. This mimics the typical laser scan strategy in which a part's contour is scanned first after which the core is infilled by hatching. The gauge section of type B is built by a hatch infill pattern surrounded by three skin passes printed at higher energy density. Hence, type B specimens exhibit defects in the outer contour region of the gauge section significantly larger than type A hatch defects. Surface and sub-surface defects in the gauge section (types C and D) are built similarly but with a single and two skin passes, respectively, at an even higher energy density. Finally, specimen types E and F are designed to exhibit entrapped-gas defects by printing the core region with a hatch infill pattern at higher energy densities. Two overheat settings (low and high) are used to generate different keyhole defect sizes.

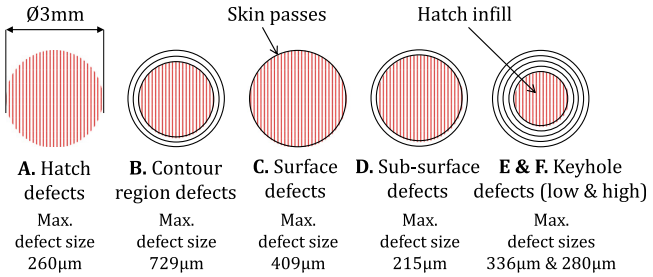

Fig. 2. Intentionally designed defects present in the gauge section of the six specimen types including max. detected defect size by XCT.

A summary of the intentionally designed defects present in the gauge section after heat treatment, machining and polishing is shown in Fig. 2. The figure also shows the maximum defect size that was detected using XCT of one specimen of each specimen type. The expectation is that a larger maximum defect size will lead to a shorter fatigue life. However, literature has shown that the largest initial defect does not always lead to the killer defect and part failure [12,13]. Also, internal defects are less prone to initiate fatigue cracks compared to surface-breaking defects [14]. Hence, next to the defect size itself, the applied scan strategies of the six specimen types will provide better insight into the fatigue failure mechanism.

The fatigue life of all 78 test specimens, 13 of each type, was determined using a Schenck fatigue test rig. The specimens were subjected to a force-controlled, tension-tension constant amplitude axial loading condition with a fatigue stress ratio ($R = S_{min}/S_{max}$) of 0.1. The UTS of similar AlSi10Mg specimens fabricated on the same machine after stress relieve is 247 MPa. The maximum stress (S_{max}) was set between 40% and 80% of this value with the majority of tests (i.e. nine for each type) at S_{max} = 140 MPa. The number of cycles to failure was recorded for each specimen up to a maximum of 5 million cycles. Run-out occurred in five instances. These five specimens were taken out of further analyses, leaving 73 test specimens in the observation group.

After specimen failure, each fracture surface was investigated using optical microscopy. The initial defect at the crack nucleation site leading to specimen failure was located and analysed. Although the 3D defect shape influences the stress concentration [15], the defect size is an accepted first-order parameter controlling the fatigue limit [16]. The major axis of the observed defect was recorded as the initial defect size. To formulate a function to evaluate the life expectancy, the S–N curve is expressed as a function of a pivot point and slope. As the S–N curve is double logarithmic, predicted life can be expressed as:

$$N_{pred} = N_{pivot} \cdot \left(\frac{S_{\max}}{S_{pivot}}\right)^{n} \text{ with } n = a \cdot d^{b} \quad (2)$$

where, N_{pred} is the predicted life in cycles to failure for an applied maximum stress of S_{max}. The subscript pivot refers to the pivot point that needs to be determined. Finally, the slope n of the S–N curve is a power law function of the defect size d and two to-be-optimized fit parameters a and b.

Both the pivot point and slope need to be determined based on experimental data. The method proposed in this paper is explained in Fig. 3.

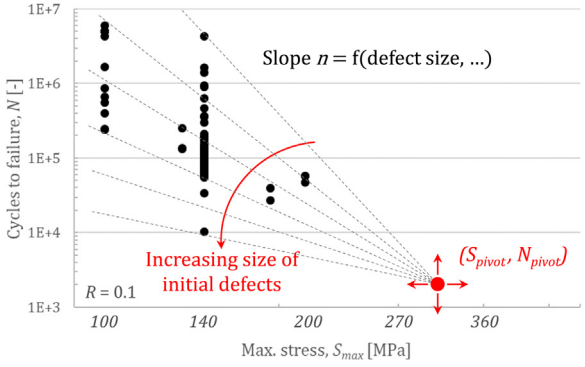

Fig. 3. Fatigue prediction where at the pivot point initial defects are assumed insignificant and the slope is a measure for the initial defect size.

Here, according to common practice, the independent (predictor) variable is represented on the *x*-axis, in this case the maximum stress the specimens are exposed to. The observed number of cycles to failure (response variable) is indicated on the *y*-axis. To quantify Eq. (2) the following steps need to be undertaken.

First, a pivot point needs to be found where the defect size is assumed insignificant in relation to the fatigue life performance. In this method, the pivot point (S_{pivot}, N_{pivot}) is a fit parameter related to a point in the *S*–*N* graph, as illustrated in Fig. 3. As initial defect sizes are assumed irrelevant, all *S*–*N* curves should go through the pivot point and hence all measured specimens are used to find the location of the pivot point.

Second, for a given pivot point, the slope between the applied maximum stress & measured fatigue life (S_{max}, N_{meas}) and the pivot point can be computed for each specimen according to:

$$n = \frac{\log_{10}(N_{meas}) - \log_{10}(N_{pivot})}{\log_{10}(S_{\max}) - \log_{10}(S_{pivot})} \quad (3)$$

The measured initial defect size is assumed to be correlated to the slope of Eq. (2). By regression analysis of this power law relation, the fit parameters *a* and *b* are determined. These fit parameters have no physical meaning and are statistically determined from the experimental data.

Third, for a given pivot point and subsequently determined fit parameters, the fatigue life of each specimen can be predicted according to Eq. (2) based on the initial defect size of each specimen. The predicted and measured life of each specimen is compared and again a regression analysis is performed. As both values should be equal, the regression is expected to result in a linear relation with both the proportionality constant and exponent equal to unity. Any deviation from unity can be adjusted by: (i) adjusting the pivot point and accordingly finding the fit parameters *a* and *b*, or (ii) expelling outliers from the statistical data set. Both corrections are performed in an iterative process in which the difference between both the proportionality constant & the exponent and unity is minimized.

3. Results and discussion

Following the aforementioned iterative process, the optimal pivot point was found to be at a stress of 310 MPa and 2000 cycles to failure. Fig. 3 actually presents all measured specimens as black dots with a majority of tests performed at 140 MPa. The pivot point is projected at 310 MPa and 2000 cycles to failure. The number of cycles is higher than for the S_{1000} method. Also, the stress is above the UTS. This can be explained by the fact that the S_{1000} method is a predictor for steel materials assuming a fully reversed stress ($R = -1$), while here aluminium is examined under net tension loading conditions ($R = 0.1$). Nevertheless, the concept of the pivot point remains similar: a point where the initial defect size has no influence on fatigue life.

For each test specimen, the resulting slope is correlated to the measured initial defect size on the fracture surface. This is shown in Fig. 4, in which each tested specimen is represented by a black dot. Four outliers are shown by the red dots. These specimens fall outside a 6σ statistical distribution range of the predicted life, as will be shown and discussed later.

The resulting power law relation of the slope of Eq. (2) is found using linear regression with parameters *a* and *b* being 25.36 and −0.27, respectively. The coefficient of determination R^2, providing a measure for the fit quality, is in this case 79%.

With Eq. (2) established, the predicted life can be computed for each specimen based on the initial defect size and its specific loading condition (S_{max}). This is shown in Fig. 5, in which the measured fatigue life is plotted as a function of the predicted fatigue life. As aforementioned, by iterating the pivot point, the proportionality constant and exponent of the linear regression line are adjusted. At the optimal pivot point location of (310, 2000), the proportionality constant and exponent are 1.01 and 1.00, respectively. Both are close to unity and the difference between measured and predicted life is minimal. As aforementioned, four outliers were removed during the iteration process.

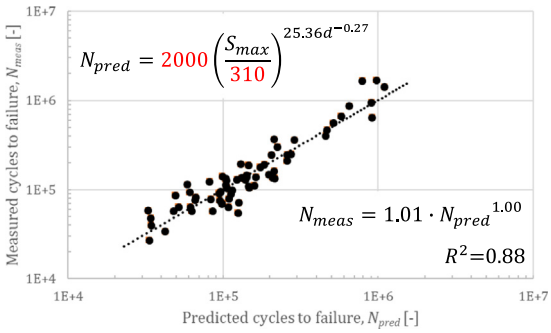

Fig. 5. Correlation between predicted and measured life with a proportionality constant and exponent of almost unity.

Certainly, a distribution of results remains due to variability in the material, specific microstructure around defect locations, exact (3D) shape of defects and proximity of other defects [7,17]. The measurement results of the test specimens are hence used for further statistical analysis. The ratio between the measured fatigue life of each specimen and its predicted value based on the initial defect size and optimal pivot point is represented in the histogram shown in Fig. 6. The average value of the differences is nearly zero ($\mu = -0.003$), illustrating that a good regression between measured and predicted life was obtained. The bin size of the histogram was set to half the standard deviation ($\sigma = 0.14$). The dotted line indicates a normal distribution. The ±3σ distribution around the mean should account for 99.73% of observations. In this case, all measurements of Fig. 5 fall within the 6σ distribution range, although four outliers were excluding during the iteration process of finding the optimal pivot point. These outliers are discussed next.

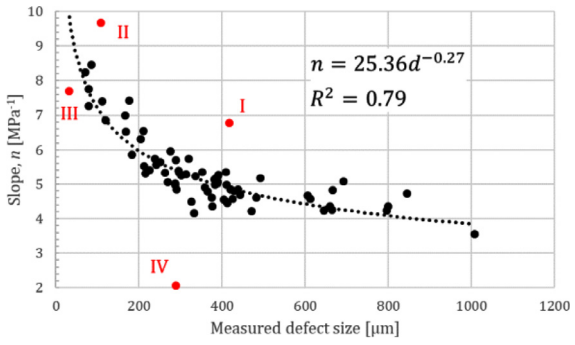

Fig. 4. Correlation between *S*–*N* curve's slopes and measured defect sizes based on a pivot point at 310 MPa and 2000 cycles to failure.

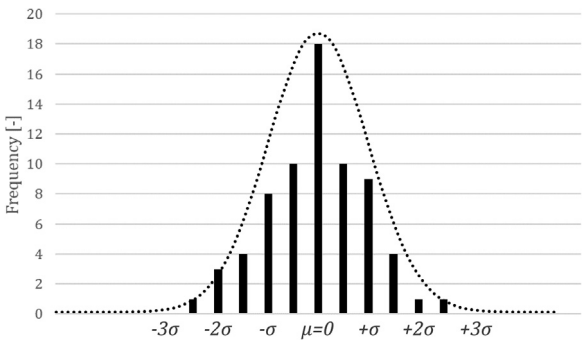

Fig. 6. Histogram of deviation between predicted and measured life.

The statistical results can also be projected onto Fig. 5. This is shown in Fig. 7. The $\pm 3\sigma$ distribution limits are indicated by the dashed lines and form a 6σ confidence interval around the mean. All specimens that were taken into account in formulating Eq. (2) fall within the 6σ distribution range. The insets illustrate that for a range of initial defect sizes (see Fig. 4), fatigue life can be predicted well. The four outliers are indicated by the red dots and clearly fall outside the confidence interval.

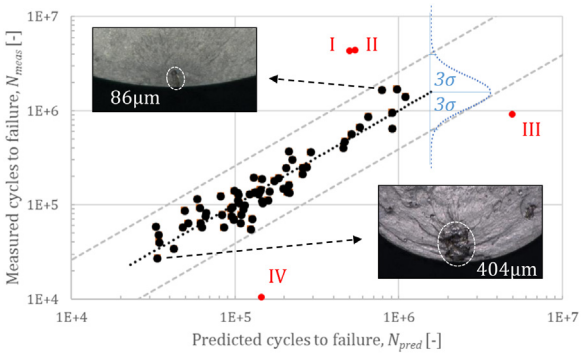

Fig. 7. Statistical analysis projected onto the predicted vs. measured life correlation; insets show fracture surfaces including initial defect size.

Outliers I and II show a much higher life than predicted based on the initial defect size. Optical microscopy revealed a defect size of 417 μm and 109 μm for outliers I and II, respectively, as shown in Fig. 8. Outlier I was part of the sub-surface defects specimen type D, while outlier II was part of the hatch defect type A. The difference in part quality can clearly be distinguished from both images. As expected, outlier I shows sub-surface defects that follow the specimen's contour, while outlier II shows a more void-free surface. The fact that these two outliers performed much better than predicted may be attributed to favourable conditions near the initial defect; e.g. favourable grain orientations and boundaries of the microstructure, and internal crack nucleation and growth without exposure to the environment.

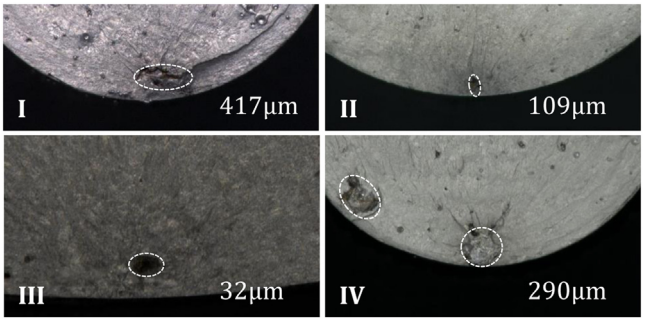

Fig. 8. Microscopic images of fractures surfaces of the four outliers.

Outliers III was also part of the hatch defect type A. The fracture surface shows little defects similar to outlier II (also type A). The specimen failed after 900,114 cycles. However, based on the initial defect size of 32 μm, the specimen was expected to last about 5 million cycles. Here, the initial defect could have been at an unfavourable position or the microstructure in proximity of the defect could have had an adverse influence on the local stress field. In any case, detecting an initial defect with such small defect size a priori for instance by XCT is not trivial. This may be a concern and call for regular inspection during a service life. The service interval may be set using the outcome of Eq. (2).

Finally, outlier IV performed very poor with only 10,338 cycles to failure. Also, the low slope, see Fig. 4, already gave an indication of poor performance. The specimen belonged to the keyhole defects type E group and had a defect size of 290 μm. However, as shown in Fig. 8, in this case there was another defect of a similar size in the same x–y plane of the specimen. This likely led to additional stress amplification, crack interaction & merger and hence extremely low fatigue performance.

4. Conclusions

A method is presented to predict the fatigue life of LPBF parts based on the assessment of an initial defect size and the applied maximum (cyclic) stress. Based on empirical data, stress-life S–N curves are fit through a pivot point, where defect sizes are assumed insignificant for fatigue life. Fatigue life predictions correlate well with experimental results. Outliers distinctly fall outside the 6σ confidence interval and may be classified as such following this method. This study showed over- as well as underperforming outliers. Even under optimal process conditions, underperforming outliers with an initial defect size as small as 32 µm may be present as inherent LPBF defect. In a critical application, such outliers should be identified by quality control or inspection measures during life.

Next to building further empirical confidence, acceptance of LPBF specifically for critically-loaded components still requires the formulation of additional modification factors taking part geometry and other stress raisers into account similar to the industry-accepted S_{1000} method. Freeform LPBF parts may not be polishable in all locations, calling for appropriate knock-down factors to assess part integrity.

Declaration of Competing Interest

The authors declare that they have no known competing financial interests or personal relationships that could have appeared to influence the work reported in this paper.

References

[1] Thompson MK, et al. (2016) Design for Additive Manufacturing: Trends, Opportunities, Considerations, and Constraints. *CIRP Annals* 65(2):737–760.
[2] Vaneker T, et al. (2020) Design for Additive Manufacturing: Framework and Methodology. *CIRP Annals* 69(2):578–599.
[3] Sanaei N, Fatemi A (2021) Defects in Additive Manufactured Metals and Their Effect on Fatigue Performance: A State-of-the-Art Review. *Progress in Materials Science* 117:100724.
[4] Ghiotti A, et al. (2022) Ti6Al4V Titanium Alloy Fatigue Strength After AM- and Machining-Based Process Chains. *CIRP Annals* 71(1):461–464.
[5] Wits WW, Scolaro E, Amsterdam E, Clare AT (2022) The Role of Scan Strategies in Fatigue Performance for Laser Powder Bed Fusion. *CIRP Annals* 71(1):185–188.
[6] Bao J, et al. (2020) Defect Evolution During High Temperature Tension-Tension Fatigue of SLM AlSi10Mg Alloy by Synchrotron Tomography. *Materials Science and Engineering: A* 792:139809.
[7] Romano S, et al. (2018) Fatigue Properties of AlSi10Mg Obtained by Additive Manufacturing: Defect-Based Modelling and Prediction of Fatigue Strength. *Engineering Fracture Mechanics* 187:165–189.
[8] Du Plessis A, et al. (2022) Fatigue Performance of Shelled Additively Manufactured Parts Subjected to Hot Isostatic Pressing. *Additive Manufacturing* 51:102607.
[9] Bannantine JA, Comer JJ, Handrock JL (1990) *Fundamentals of Metal Fatigue Analysis*, Prentice HallEnglewood Cliffs, NJ.
[10] McKelvey SA, Fatemi A (2012) Surface Finish Effect on Fatigue Behavior of Forged Steel. *International Journal of Fatigue* 36(1):130–145.
[11] Brandl E, Heckenberger U, Holzinger V, Buchbinder D (2012) Additive Manufactured AlSi10Mg Samples Using Selective Laser Melting (SLM): Microstructure, High Cycle Fatigue, and Fracture Behavior. *Materials & Design* 34:159–169.
[12] Persenot T, et al. (2020) Fatigue Performances of Chemically Etched Thin Struts Built by Selective Electron Beam Melting: Experiments and Predictions. *Materialia* 9:100589.
[13] McMurtrey MD, Mills DE, Burns JT (2019) The Effect of Pit Size and Density on the Fatigue Behaviour of a Pre-Corroded Martensitic Stainless Steel. *Fatigue & Fracture of Engineering Materials & Structures* 42(1):3–18.
[14] Serrano-Munoz I, et al. (2017) Location, Location & Size: Defects Close to Surfaces Dominate Fatigue Crack Initiation. *Scientific Reports* 7(1):45239.
[15] Nicoletto G, Konečná R, Fintova S (2012) Characterization of Microshrinkage Casting Defects of Al–Si alloys by X-ray Computed Tomography and Metallography. *International Journal of Fatigue* 41:39–46.
[16] Domfang Ngnekou JN, et al. (2019) Fatigue Properties of AlSi10Mg Produced by Additive Layer Manufacturing. *International Journal of Fatigue* 119:160–172.
[17] Tammas-Williams S, Withers PJ, Todd I, Prangnell PB (2017) The Influence of Porosity on Fatigue Crack Initiation in Additively Manufactured Titanium Components. *Scientific Reports* 7(1):7308.